

**Possible half-metallic antiferromagnetism in an iridium double-perovskite material**

Madhav Prasad Ghimire, Long-Hua Wu, and Xiao Hu\*

*International Center for Materials Nanoarchitectonics (WPI-MANA), National Institute for Materials Science, Tsukuba 305-0044, Japan*

(Received 3 June 2014; revised manuscript received 15 March 2016; published 19 April 2016)

Using the first-principles density functional approach, we investigate a material  $\text{Pr}_2\text{MgIrO}_6$  (PMIO) of double-perovskite structure synthesized recently. According to the calculations, PMIO is a magnetic Mott-Hubbard insulator with  $\mu_{\text{tot}} \simeq 6\mu_B$  per unit cell influenced by the cooperative effect of spin-orbit coupling (SOC) and Coulomb interactions of Ir- $5d$  and Pr- $4f$  electrons, as well as the crystal field. When Pr is replaced with Sr gradually, the system exhibits half-metallic (HM) states desirable for spintronics applications. In  $[\text{Pr}_{2-x}\text{Sr}_x\text{MgIrO}_6]_2$ , HM antiferromagnetism (HMAFM) with zero magnetic moment in the unit cell is obtained for  $x = 1$ , whereas for  $x = 0.5$  and  $1.5$  HM ferrimagnetism (HMFIM) is observed with  $\mu_{\text{tot}} \simeq 3\mu_B$  and  $\mu_{\text{tot}} \simeq -3\mu_B$  per unit cell respectively. It is emphasized that the large exchange splitting between spin-up and spin-down bands at the Fermi level makes the half-metallicity possible even with strong SOC.

DOI: [10.1103/PhysRevB.93.134421](https://doi.org/10.1103/PhysRevB.93.134421)**I. INTRODUCTION**

Half-metals (HMs) are a class of materials which are metallic in one spin channel while insulating in the opposite spin channel, due to the asymmetric band structure [1–7]. HMs can generate spin-polarized currents without any external operation, and thus are very useful for spintronics applications. They have been identified in several groups of materials [8–16] and huge magnitudes of magnetoresistance have been reported [17]. It was noted, however, that spin-polarized current might be hampered by stray fields which stabilize magnetic domains. This drawback can be overcome in HM antiferromagnets (HMAFM), a subclass of HMs characterized further by zero spin magnetization per unit cell [2,7]. A brand new field coined *antiferromagnetic spintronics* is emerging that involves exploration of novel functionalities of antiferromagnets [18–20].

Ideally HM in a stoichiometric material is a quantum state specified by integer spin magnetization in units of Bohr magneton ( $\mu_B$ ) per unit cell, where all valence bands are fully filled in the insulating spin channel. In reality, however, accurate integer spin magnetization has hardly been achieved. An apparent reason is the quality of a crystal. Another, and more intrinsic, reason may be the existence of spin-orbit coupling (SOC), which is especially important for heavy elements.

Generally speaking, SOC is taken as an unfavorable effect for spintronic applications, in which one wishes to keep the spin moment for information processing and encoding. A naive question then arises of whether HM can survive in the presence of sizable SOC. In the presence of other fields, the answer to this question can be positive. Actually, it is revealed that a topological HMAFM state can be generated by simultaneous application of antiferromagnetic exchange field and alternating electric potential in addition to SOC in a double-perovskite structure [21]. Generalizing the idea into broader classes of materials is expected to provide a new facet for developing functional materials. A newly synthesized double-perovskite material,  $\text{Pr}_2\text{MgIrO}_6$  (PMIO) [22], attracts our attention with unique properties: Pr atoms and Ir atoms carry opposite

magnetic moment, and oxygen octahedra exhibit large crystal distortion, which may induce strong crystal fields and help split the spin-up and spin-down bands, which are expected to compete with the strong SOC in Ir and Pr atoms.

It is also worth noticing that iridates themselves have been attracting significant interest recently, which yield various unconventional phases in cooperation with the strongly correlated effects due to Coulomb interaction among electrons. For instance,  $\text{Sr}_2\text{IrO}_4$  has been evidenced by an experiment to be a  $J_{\text{eff}} = 1/2$  Mott insulator [23–25].  $\text{Ln}_2\text{Ir}_2\text{O}_7$  is predicted to transform from a topological band insulator to a topological Mott insulator [26]. The topological semimetal state has been predicted in  $\text{Y}_2\text{Ir}_2\text{O}_7$ , characterized by Fermi arcs on surface [27].

We have performed first-principles density-functional-theory (DFT) calculations on PMIO. It is found that PMIO is a Mott-Hubbard insulator, where a Pr atom carries approximately  $2\mu_B$  magnetic moment, while Ir atoms and oxygen atoms carrying negative magnetic moments, resulting in  $\mu_{\text{tot}} \simeq 6\mu_B$  per unit cell. This material is interesting in the sense that (i) the topmost valence states close to Fermi level ( $E_F$ ) are exclusively up-magnetic-moment bands contributed from  $d$  electrons of Ir, and (ii) the  $A$ -site element Pr provides both charge and magnetic moment as opposed to most perovskite materials. Therefore, holes doped into the system tend to exhibit up magnetic moment, which makes this material a unique platform for material tailored with simultaneous control on charge and spin. Specifically, we consider the replacement of Pr by Sr, with Sr being nonmagnetic and donating one electron less than Pr. We find that the material  $[\text{Pr}_{2-x}\text{Sr}_x\text{MgIrO}_6]_2$  is HMFIM with  $\mu_{\text{tot}} \simeq 3\mu_B$  and  $-3\mu_B$  at  $x = 0.5$  and  $1.5$  respectively, and HMAFM with  $\mu_{\text{tot}} = 0$  at  $x = 1$ . The interplay among Coulomb repulsion, SOC, and the crystal field plays an important role in this material. To the best of our knowledge, this is the first prediction of HMAFM with large SOC.

**II. CRYSTAL STRUCTURES AND METHODS**

The crystal structure of PMIO is shown in Fig. 1(a), which falls in the space group  $P2_1/n$  derived from the double-perovskite structure. It has monoclinic structural distortion

\*Hu.Xiao@nims.go.jp

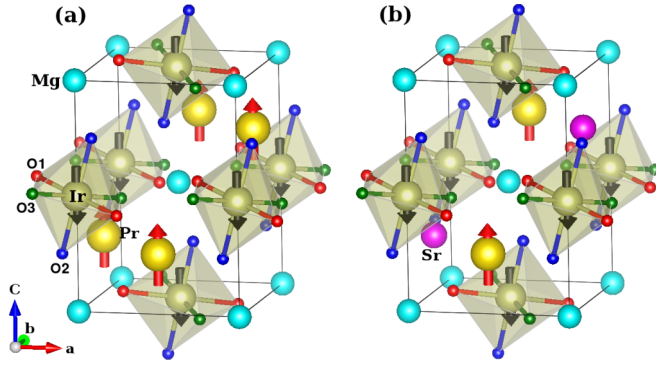


FIG. 1. Crystals of double-perovskite structure: (a) parent material  $[\text{Pr}_2\text{MgIrO}_6]_2$ ; (b) material with half Pr replacement  $[\text{PrSrMgIrO}_6]_2$ . The red (black) arrows indicate the direction of Pr (Ir) spins along the  $c$  direction, which is the easy axis.

due to the tilting and rotation of  $\text{IrO}_6$  octahedron to maintain favorable Pr-O distances [22]. In addition, there are three sorts of oxygen positions with Ir-O bond lengths  $l_x = 2.06 \text{ \AA}$ ,  $l_y = 2.02 \text{ \AA}$ , and  $l_z = 2.01 \text{ \AA}$ , respectively [see Fig. 2(b)], which reduces the cubic symmetry  $O_h$  and lifts the degeneracy of Ir- $d$  orbitals. The longest bond  $l_x$  weakens the repulsion between ligand electrons and the Ir- $d$  orbitals along this direction, and thus the  $d_{yz}$  orbital takes a higher energy than the  $d_{xz}$  and  $d_{xy}$  orbitals. Similarly, the energy of  $d_{xz}$  is slightly higher than  $d_{xy}$  since  $l_z < l_y$ .

In order to provide a realistic description of the electronic and magnetic structures, a set of first-principles DFT calculations were performed using the full-potential linearized augmented plane wave plus local orbital method implemented in the WIEN2K code [28]. The size of muffin tin  $R_{\text{MT}}$  is 2.44, 2.2, 1.91, 2.07, and 1.7 Bohr radius for Pr, Sr, Mg, Ir, and O respectively. A set of 2000  $k$ -points were used in the full Brillouin zone. The standard generalized-gradient

approximation (GGA) exchange-correlation potential within the PBE scheme [29] was used with Coulomb interaction  $U$  [30]. The results shown here are for  $U_{\text{Pr}} = 5 \text{ eV}$  and  $U_{\text{Ir}} = 1.25 \text{ eV}$  [31], and we have confirmed that the results remain unchanged in a reasonable ranges  $U_{\text{Pr}} \leq 8 \text{ eV}$  and  $U_{\text{Ir}} < 2 \text{ eV}$ . Spin-orbit coupling is considered via a second variational step using the scalar-relativistic eigenfunctions as basis [32]. Starting from the lattice parameters given by experiments [22], we relax the lattice and reach the stable structure using the VASP package [33] with the force convergence set at  $0.01 \text{ eV/\AA}$ . The on-site Coulomb interactions are treated by Dudarev's method [34]. We use an  $8 \times 8 \times 8$   $k$ -point mesh within the Monkhorst-Pack scheme [35] with energy cutoff  $400 \text{ eV}$ . We confirm that the results remain unchanged for a cutoff energy  $600 \text{ eV}$ .

### III. PARENT MATERIAL $[\text{Pr}_2\text{MgIrO}_6]_2$

The same as most  $A$ -site elements in perovskite materials, in PMIO Pr provides charge to the system and nominally takes the charge state  $+3$  with  $4f^2$  configuration lying deeply in the valence band. Unlike other cases, however, Pr is in a high-spin state due to strong Hund's coupling. The transition element Ir nominally takes the charge state of  $+4$  with  $5d^5$  configuration, where five of the six  $t_{2g}$  orbitals are occupied and lie at the top of the valence band, forming a low-spin state due to large crystal field from the oxygen octahedron. According to first-principles calculations, there is an energy gap of  $\sim 0.2 \text{ eV}$  at  $E_{\text{F}}$  (see Fig. 2) indicating clearly that PMIO is a Mott-Hubbard insulator. There is no experimental report on the energy gap of PMIO; however, its isovalent compound  $\text{La}_2\text{MgIrO}_6$  has been identified to have a similar crystal structure with AFM ground state and a Mott-insulating state (experimental band gap is  $0.16 \text{ eV}$ , which was well reproduced by first-principles calculations using  $U_{\text{Ir}} = 1.25 \text{ eV}$  [31]. Based on the above value of  $U$ , PMIO is predicted to be an insulator.

As revealed by the partial density of states (PDOS) in spin-up and spin-down channels [37] and the band structures obtained from first-principles calculations as well as Wannier downfolding analyses (Fig. 2), the  $t_{2g}$  orbitals splits into  $d_{yz} > d_{xz} \geq d_{xy}$  in the order of energy, and a large exchange energy  $\sim 1.2 \text{ eV}$  pushes those in the spin-down channel away from  $E_{\text{F}}$ . This is caused by distortions of octahedron in the present material, where there are three sorts of oxygen positions with different Ir-O bond lengths  $l_z \leq l_y < l_x$  (see the appendix for a discussion on hopping integrals among  $t_{2g}$  orbitals obtained by Wannier downfolding scheme in  $[\text{Pr}_2\text{MgIrO}_6]_2$ ). The contributions from Pr- $4f$  states (dominated by  $f_{5xz^2-xr^2}$  and  $f_{z^2-x^2-y^2}$ ) are negligible and has the least effect near  $E_{\text{F}}$ .

The magnetic property of PMIO is of particular interest. At the ground state obtained from first-principles calculations, Pr couples antiferromagnetically with Ir. The calculated total magnetic moment ( $\mu_{\text{tot}}$ ) is  $6.02\mu_{\text{B}}$  per unit cell (see Table I), which is slightly larger than the experimental value of  $\mu_{\text{tot}} = 5.16\mu_{\text{B}}$  [22]. In an ionic picture, each Pr ion carries moment  $+2\mu_{\text{B}}$  while Ir ion carries  $-1\mu_{\text{B}}$ , giving rise to  $\mu_{\text{tot}} = 4 \times (+2\mu_{\text{B}}) + 2 \times (-1\mu_{\text{B}}) = 6\mu_{\text{B}}$  in a unit cell, consistent with the first-principles calculations.

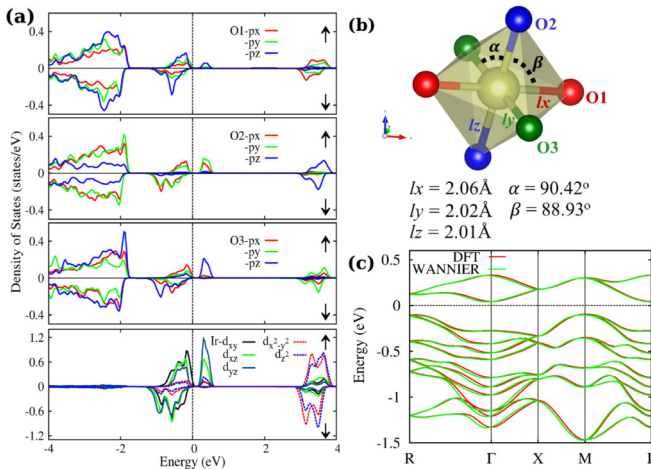


FIG. 2. (a) Partial density of states for three inequivalent oxygen- $2p$  states and Ir- $5d$  states in spin-up ( $\uparrow$ ) and spin-down ( $\downarrow$ ) channels, (b) a distorted  $\text{IrO}_6$  octahedron, and (c) band structure with red (green) curves for results based on the DFT (Wannier) [36] method for the parent material  $[\text{Pr}_2\text{MgIrO}_6]_2$ .

TABLE I. The magnetic moments including spin and orbital contributions per atom of Pr and Ir, per set of three inequivalent oxygen atoms, and per unit cell respectively for  $[\text{Pr}_{2-x}\text{Sr}_x\text{MgIrO}_6]_2$  from first-principles calculations. The unit of moments is the Bohr magneton  $\mu_B$ . The contributions from individual atoms are within muffin tins while the total magnetic moment includes those from interstitial regime.

$x$	Pr	Ir	O	$\mu_{\text{tot}}$
0	1.98	-0.55	-0.22	6.02
0.5	1.97	-0.76	-0.32	3.07
1	1.96	-0.98	-0.43	0.08
1.5	1.96	-1.17	-0.58	-2.97

#### IV. DOPED MATERIALS $[\text{Pr}_{2-x}\text{Sr}_x\text{MgIrO}_6]_2$

The above properties of PMIO make it a promising candidate for exploring possible HM states. To be specific, we consider the *A*-site modification by replacing Pr with Sr, a nonmagnetic element usually of +2 charge state, which corresponds to hole doping into the parent material. Presuming that the overall magnetic configuration will not be changed upon replacement, a hole will go to the spin-up channel and reduce the total magnetic moment by  $\mu = 3\mu_B$ , with  $2\mu_B$  taken away by the replaced Pr atom and  $1\mu_B$  due to  $E_F$  shift. In this way, one can modify the material with fine control on both spin and charge.

We perform first-principles calculations to check the above idea. Let us focus on the most interesting case of replacement rate  $x = 1$ , where two Pr atoms are replaced by two Sr atoms, and thus two holes are doped into the system per unit cell. From the view of rigid band model, doping hole shifts  $E_F$  downward to the valence region such that it crosses the topmost occupied states. As revealed by first-principles calculations,

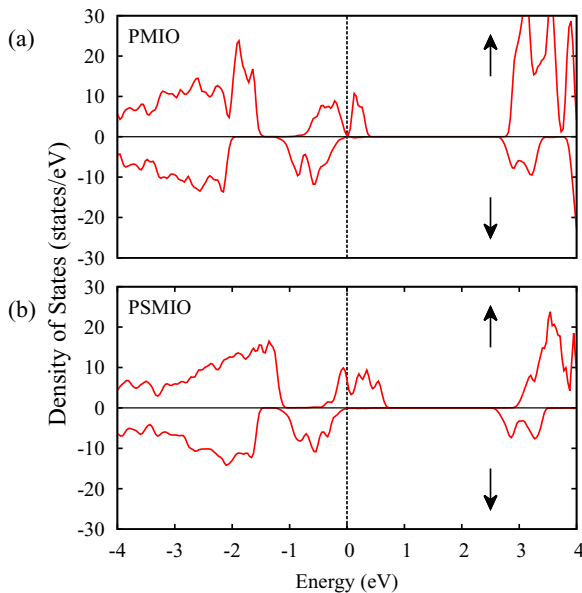


FIG. 3. Total density of states obtained by GGA +  $U$  + SOC scheme for spin-up ( $\uparrow$ ) and spin-down ( $\downarrow$ ) channels: (a) parent material  $[\text{Pr}_2\text{MgIrO}_6]_2$ , (b) material with half Pr replacement  $[\text{PrSrMgIrO}_6]_2$ .

the two holes from Sr go to the spin-up Ir- $d_{xz}$  states that lie just below  $E_F$  in the parent material, and push them up above  $E_F$ . The spin-down channel remains insulating since no change occurs in the valence states. With spin-up channel metallic and spin-down channel insulating, the system turns to a HM as clearly seen in Fig. 3(b). Figure 4 shows the partial DOS contribution from Pr-4*f*, Ir-5*d*, and oxygen-2*p* states. It is noted that the occupied Pr-4*f* states lie deep in the valence region for spin-up channel, whereas for spin-down channel they appear far from  $E_F$  in the conduction region. This gives rise to large exchange energy splitting ( $\sim 6$  eV) in Pr. It is clear that in spin-up channel the Ir- $t_{2g}$  orbits originally in the valence band are now pushed up to cross  $E_F$  and form a continuous band there. Oxygen *p* orbits also appear around  $E_F$  due to the hybridization with Ir *d* electrons.

As summarized in Table I, two replaced Pr atoms take away  $\mu \simeq 4\mu_B$ , and the shift of  $E_F$  associated doped two holes in the spin-up channel contributes a reduction of  $\mu \simeq 2\mu_B$  further, which reduces the total magnetic moment to zero. These features can also be seen from the spin-density isosurface plot in Fig. 5. With the zero total magnetic moment and HM property, we conclude that the material  $\text{PrSrMgIrO}_6$  should be a HMAFM. To the best of our knowledge, this is the first proposal for HMAFM with large SOC taken into account.

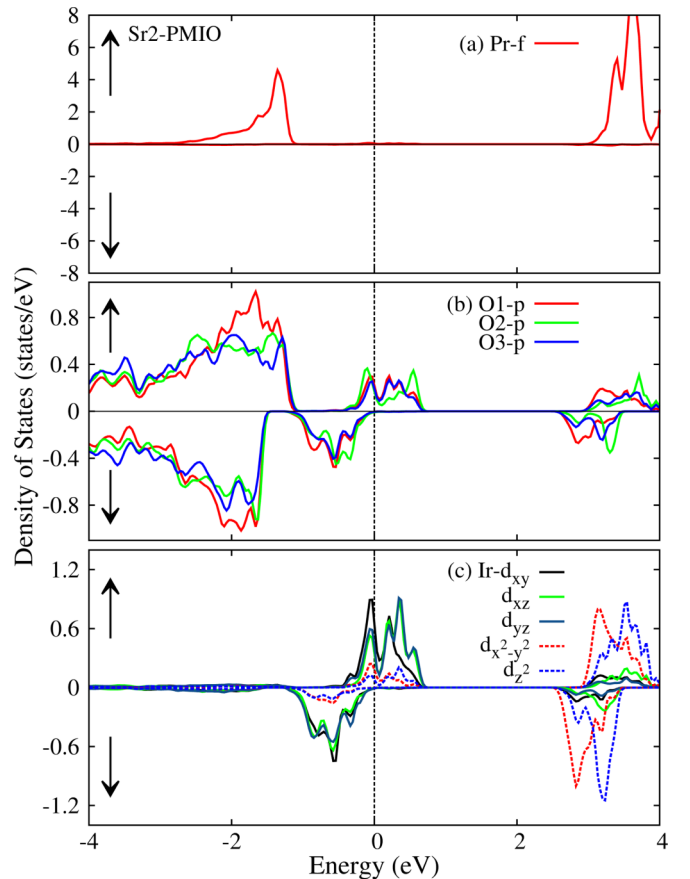


FIG. 4. Partial density of states for Pr-4*f* states, three inequivalent oxygen-2*p* states and Ir-5*d* states in spin-up ( $\uparrow$ ) and spin-down ( $\downarrow$ ) channels for material with half Pr replacement  $[\text{PrSrMgIrO}_6]_2$  (Sr2-PMIO).

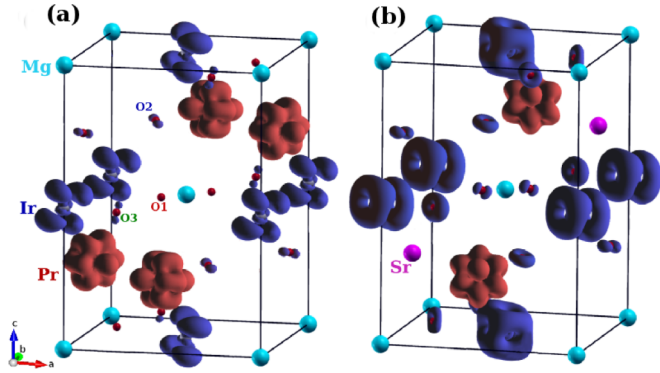


FIG. 5. Isosurface of spin magnetization density at  $\pm 0.21 e/\text{\AA}^3$  with red (blue) for spin up (down): (a) parent material  $[\text{Pr}_2\text{MgIrO}_6]_2$  and (b) material with half Pr replacement  $[\text{PrSrMgIrO}_6]_2$ .

HM states are also obtained for the replacement rates  $x = 0.5$  and  $x = 1.5$  in  $[\text{Pr}_{2-x}\text{Sr}_x\text{MgIrO}_6]_2$  (see Fig. 6) where one and/or three Pr atoms are replaced by Sr atoms per unit cell. For  $x = 0.5$ , one hole from Sr goes to the spin-up Ir- $d_{xz}$  band that was lying in the topmost valence region below  $E_F$  in the parent material. As a result, the Ir- $d_{xz}$  band shifts to the conduction region and forms a continuous band with the Ir- $d$  bands in the valence region. This gives rise to a metallic state for the spin-up channel, while valence states in the spin-down channel remain far from  $E_F$ . Similar results have been achieved for  $x = 1.5$ , except that three holes from Sr are transferred to spin-up Ir- $5d$  states. The two materials are HMFIM with  $\mu_{\text{tot}} = +3\mu_B$  and  $\mu_{\text{tot}} = -3\mu_B$  per unit cell respectively.

## V. DISCUSSIONS

In PMIO, SOC is crucially important due to the presence of heavy elements such as Pr and Ir. The orbital moments obtained

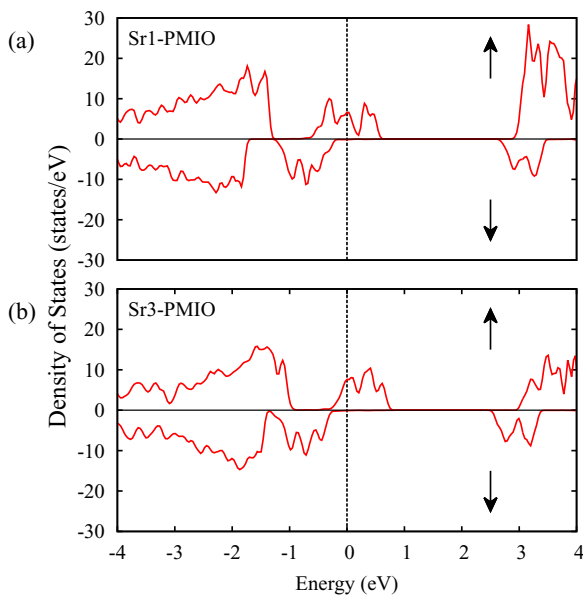


FIG. 6. Total density of states obtained for (a)  $x = 0.5$  (Sr1-PMIO) and (b)  $x = 1.5$  (Sr3-PMIO) in  $[\text{Pr}_{2-x}\text{Sr}_x\text{MgIrO}_6]_2$  in spin-up ( $\uparrow$ ) and spin-down ( $\downarrow$ ) channels.

from first-principles calculations for Pr ( $-0.4\mu_B$ ) come from  $f_{5xz^2-xr^2}$  and  $f_{zx^2-zy^2}$  while those of Ir ( $-0.2\mu_B$ ) come from the  $t_{2g}$  states. These moments are in accordance with the Hund's third rule, where Pr with less than half-filled  $f$  shell has its orbital moment antiparallel to its spin moment, whereas Ir with more than half-filled  $t_{2g}$  shell has its orbital moment parallel to its spin moment [38]. Hence the total magnetic moment decreases for Pr while it increases for Ir respectively. For the case of  $[\text{PrSrMgIrO}_6]_2$ , the orbital moment of Ir becomes weaker due to charge transfer effect. Hence zero effective moment is achieved even when SOC is considered. The magnetic moments, which are the summation of spin and orbital moments from individual atoms, are summarized in Table I.

Charge-transfer effects [39] are prominent between Ir and oxygen, especially in O2 and O3 due to their shorter bond lengths with Ir, which takes place between O2 and Ir via  $p_x$ ,  $p_y$  and  $d_{xz}$ ,  $d_{yz}$  states, and between O3 and Ir via  $p_z$  and  $d_{xz}$ ,  $d_{yz}$  states. In order to accommodate charge transfers from Ir atoms carrying spin-up polarization (spin-down channel is fully occupied), the spin-up channel of oxygen  $p$  orbitals is left partially occupied with the spin-down channel fully occupied. This yields excess spin-down electrons at oxygen, which results in a FM coupling between Ir and O as shown in Table I [see also Fig. 5(a)].

Doping holes enhance the spin moment further at Ir and oxygen [see Fig. 5(b)]. Similar features were reported for Sr-doped  $\text{LaCoO}_3$  [40]. First-principles calculations on magnetic anisotropy energy indicates that the  $c$  axis of the crystal as the easy axis (see Fig. 1) with anisotropy energy of  $\sim 27$  meV per unit cell for the parent material.

It is well known that SOC mixes spin-up and spin-down bands, and thus spin-polarization at  $E_F$  may be affected. It is not the case for the present materials, where the exchange splitting between the spin-up and spin-down DOS at  $E_F$  is large (see Fig. 3) and the mixing does not happen despite the strong SOC ( $\sim 0.35$  eV) [41]. This is the first theoretical prediction of HMAFM based on first-principles calculations involving strong SOC.

In order to check the robustness of half-metallicity in the present materials, we consider the disorder effects. There are two main types of disorders, known as antisite disorder [42], where the positions of Mg and Ir atoms at  $B$  and  $B'$  sites are interchanged, and cation disorder where Sr atoms replace Pr atoms at different  $A$ -site positions. We have confirmed that the HMAFM remains stable in the disordered configurations. Shown in Fig. 7 are two examples of antisite disorder (b) and

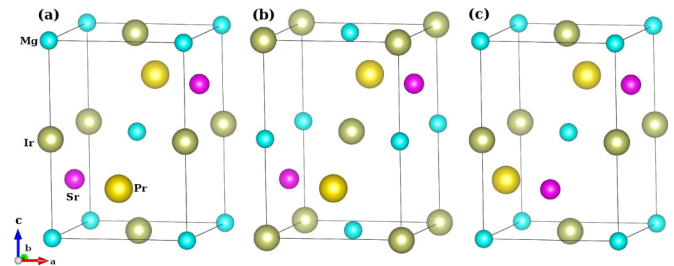


FIG. 7. Configuration of ground state (a), lowest-excitation state in antisite disorder (b), and cation disorder (c) for the material  $[\text{PrSrMgIrO}_6]_2$ . Oxygen atoms are not shown for clear view.

cation disorder (c) for the replacement rate  $x = 1$ , which are the lowest excited states to the ground state with excitation energy of 400 and 70 meV respectively.

In the present work, HMAFM and HMFIM have been derived from the same parent material. Thus, using them in an integrated system, one can construct a useful device for spintronics applications without suffering from the problem of lattice mismatching.

## VI. CONCLUSIONS

Based on the first-principles density functional approach, we propose material tailoring a Mott-Hubbard insulator  $\text{Pr}_2\text{MgIrO}_6$  with double-perovskite structure, exploiting the cooperative effect from Coulomb interaction, spin-orbit coupling, and the crystal field. It is demonstrated that by doping holes into the system by replacing Pr with Sr, one can achieve several half-metals. Especially,  $\text{PrSrMgIrO}_6$  is found to be a half-metallic antiferromagnet, namely half-metal with zero magnetic moment per unit cell, which is ideal for spintronics. It is emphasized that the large exchange splitting between spin-up and spin-down bands at the Fermi level retains the half-metallicity even in the presence of strong spin-orbit coupling.

TABLE II. Transfer hopping integrals in units of meV among  $t_{2g}$  orbitals of Ir atoms at the equivalent position in unit cells. For example, the hopping integrals with (1,0,0) denote the rates of Ir- $d$  electrons hopping to the Ir atom at the equivalent position in the nearest unit cell along  $x$  axis. (0,0,0) refers to the onsite energies and interorbital couplings. The row order of  $6 \times 6$  transfer matrix is identical to that of the column. We only show the upper triangular part of self-adjoint transfer matrix.

Direction	$d_{xz}, \uparrow$	$d_{yz}, \uparrow$	$d_{xy}, \uparrow$	$d_{xz}, \downarrow$	$d_{yz}, \downarrow$	$d_{xy}, \downarrow$
0,0,0	6600	$-209 + 160i$ 6726	$73 - 11i$ $-83 - 81i$ 6435	$-5 + 9i$ $-27 - 83i$ $152 - 58i$ 6085	$31 + 58i$ $-3 + 12i$ $-48 - 130i$ $141 - 135i$ 6031	$-160 + 61i$ $62 + 127i$ 0 $54 + 6i$ $43 + 75i$ 6190
1,0,0	-7	-8 33	-19 -10 -64	0 0 0 -1	0 0 0 0 36	0 0 0 -20 -8 -68
0,1,0	-18	4 37	37 -28 -81	0 0 0 -17	0 0 0 4 44	0 0 0 39 -33 -76
0,0,1	-10	2 6	-2 3 4	0 0 0 -10	0 0 0 2 5	0 0 0 -2 2 3
1,1,0	-8	0 4	6 6 0	0 0 0 -11	0 0 0 0 3	0 0 0 7 5 1

## ACKNOWLEDGMENTS

The authors thank R. Yu for valuable discussions. This work was supported by WPI Initiative on Materials Nanoarchitectonics, Ministry of Education, Cultures, Sports, Science and Technology, Japan.

## APPENDIX: DOWNFOLDING BY WANNIER FUNCTIONS

In order to get an intuitive real-space picture on how Ir- $t_{2g}$  electrons close to Fermi level hop, we employ WANNIER90 [36] to project the bands obtained from DFT calculations to the localized Wannier functions, i.e., the Ir- $d_{xy}$ ,  $d_{xz}$  and  $d_{yz}$  orbitals. Since there are two Ir atoms in a unit cell, the total number of Wannier functions is twelve for the two spin channels. The results listed in Tables II and III are obtained by taking two unit cells as the cutoff distance in all directions. The substantial imaginary parts of the onsite interorbital coupling in Table II come from the spin-orbit coupling. As displayed in Table II, large energy differences between spin-up and spin-down electrons prevent spin-down electrons from being pulled up to Fermi level by the spin-orbit coupling. We confirm that the DFT results can be reproduced in terms of the hopping integrals up to the nearest-neighbor unit cells among the Wannier orbitals [see Fig. 2(c) in the main text].

TABLE III. Transfer hopping integrals in units of meV among  $t_{2g}$  orbitals of Ir atoms at the two inequivalent positions in unit cells. (0,0,0) refers to the hopping integrals among the two inequivalent Ir atoms in the same unit cell.  $d_{\alpha}^{1(2)}$  represents the  $d_{\alpha}$  orbital of Ir located in the middle (corner) of the  $a-b$  plane in Fig. 1(a), where  $\alpha = xy, xz, yz$ .

Direction 0,0,0	$d_{xz}^1, \uparrow$	$d_{yz}^1, \uparrow$	$d_{xy}^1, \uparrow$	$d_{xz}^1, \downarrow$	$d_{yz}^1, \downarrow$	$d_{xy}^1, \downarrow$
$d_{xz}^2, \uparrow$	-35	-55	28	0	0	0
$d_{yz}^2, \uparrow$	-46	-17	17	0	0	0
$d_{xy}^2, \uparrow$	-31	-29	26	0	0	0
$d_{xz}^2, \downarrow$	0	0	0	-37	-56	24
$d_{yz}^2, \downarrow$	0	0	0	-58	-18	24
$d_{xy}^2, \downarrow$	0	0	0	-32	-29	27
Direction 1,0,0						
$d_{xz}^2, \uparrow$	0	0	2	0	0	0
$d_{yz}^2, \uparrow$	0	-2	0	0	0	0
$d_{xy}^2, \uparrow$	2	0	3	0	0	0
$d_{xz}^2, \downarrow$	0	0	0	0	0	-2
$d_{yz}^2, \downarrow$	0	0	0	0	-2	0
$d_{xy}^2, \downarrow$	0	0	0	2	2	3

TABLE III. (Continued.)

Direction 0,0,0	$d_{xz}^1, \uparrow$	$d_{yz}^1, \uparrow$	$d_{xy}^1, \uparrow$	$d_{xz}^1, \downarrow$	$d_{yz}^1, \downarrow$	$d_{xy}^1, \downarrow$
Direction 0,1,0						
$d_{xz}^2, \uparrow$	-3	-1	0	0	0	0
$d_{yz}^2, \uparrow$	0	0	-3	0	0	0
$d_{xy}^2, \uparrow$	0	1	-3	0	0	0
$d_{xz}^2, \downarrow$	0	0	0	-3	-1	0
$d_{yz}^2, \downarrow$	0	0	0	1	2	-4
$d_{xy}^2, \downarrow$	0	0	0	-1	0	-2
Direction 0,0,1						
$d_{xz}^2, \uparrow$	12	-52	20	0	0	0
$d_{yz}^2, \uparrow$	-48	-41	-7	0	0	0
$d_{xy}^2, \uparrow$	5	-14	12	0	0	0
$d_{xz}^2, \downarrow$	0	0	0	13	-46	23
$d_{yz}^2, \downarrow$	0	0	0	-51	-47	-10
$d_{xy}^2, \downarrow$	0	0	0	0	-10	12

- [1] R. A. de Groot, F. M. Mueller, P. G. van Engen, and K. H. J. Buschow, *Phys. Rev. Lett.* **50**, 2024 (1983).
- [2] H. van Leuken and R. A. de Groot, *Phys. Rev. Lett.* **74**, 1171 (1995).
- [3] W. E. Pickett and J. S. Moodera, *Phys. Today* **54**, 39 (2001).
- [4] S. A. Wolf, D. D. Awschalom, R. A. Buhrman, J. M. Daughton, S. von Molnar, M. L. Roukes, A. Y. Chtchelkanova, and D. M. Treger, *Science* **294**, 1488 (2001).
- [5] C. Felser, G. H. Fecher, and B. Balke, *Angew. Chem., Int. Ed. Engl.* **46**, 668 (2007).
- [6] M. I. Katsnelson, Y. Yu. Irkhin, L. Chioncel, A. I. Lichtenstein, and R. A. de Groot, *Rev. Mod. Phys.* **80**, 315 (2008).
- [7] X. Hu, *Adv. Mater.* **24**, 294 (2012).
- [8] W. E. Pickett, *Phys. Rev. B* **57**, 10613 (1998).
- [9] D. D. Sarma, P. Mahadevan, T. Saha-Dasgupta, S. Ray, and A. Kumar, *Phys. Rev. Lett.* **85**, 2549 (2000).
- [10] J. H. Park, S. K. Kwon, and B. I. Min, *Phys. Rev. B* **65**, 174401 (2002).
- [11] X. Wan, M. Kohno, and X. Hu, *Phys. Rev. Lett.* **94**, 087205 (2005); **95**, 146602 (2005).
- [12] H. Akai and M. Ogura, *Phys. Rev. Lett.* **97**, 026401 (2006).
- [13] Y.-M. Nie and X. Hu, *Phys. Rev. Lett.* **100**, 117203 (2008).
- [14] G. M. Müller, J. Walowski, M. Djordjevic, G.-X. Miao, A. Gupta, A. V. Ramos, K. Gehrke, V. Moshnyaga, K. Samwer, J. Schmalhorst, A. Thomas, A. Hütten, G. Reiss, J. S. Moodera, and M. Müntenberg, *Nat. Mater.* **8**, 56 (2009).
- [15] S.-J. Hu and X. Hu, *J. Phys. Chem. C* **114**, 11614 (2010).
- [16] H. Kurt, K. Rode, P. Stamenov, M. Venkatesan, Y.-C. Lau, E. Fonda, and J. M. D. Coey, *Phys. Rev. Lett.* **112**, 027201 (2014).
- [17] Y. Tokura, *Rep. Prog. Phys.* **69**, 797 (2006).
- [18] B. G. Park, J. Wunderlich, X. Martí, V. Holý, Y. Kurosaki, M. Yamada, H. Yamamoto, A. Nishide, J. Hayakawa, H. Takahashi, A. B. Shick, and T. Jungwirth, *Nat. Mater.* **10**, 347 (2011).
- [19] Y. Y. Wang, C. Song, B. Cui, G. Y. Wang, F. Zeng, and F. Pan, *Phys. Rev. Lett.* **109**, 137201 (2012).
- [20] D. Sando, A. Agbelele, D. Rahmedov, J. Liu, P. Rovillain, C. Toulouse, I. C. Infante, A. P. Pyatakov, S. Fusil, E. Jacquet, C. Carrétéro, C. Deranlot, S. Lisenkov, D. Wang, J.-M. Le Breton, M. Cazayous, A. Sacuto, J. Juraszek, A. K. Zvezdin, L. Bellaiche, B. Dkhil, A. Barthélémy, and M. Bibes, *Nat. Mater.* **12**, 641 (2013).
- [21] Q.-F. Liang, L.-H. Wu, and X. Hu, *New J. Phys.* **15**, 063031 (2013).
- [22] S. J. Mugavero III, A. H. Fox, M. D. Smith, and H.-C. zur Loye, *J. Solid State Chem.* **183**, 465 (2010).
- [23] B. J. Kim, H. Jin, S. J. Moon, J.-Y. Kim, B.-G. Park, C. S. Leem, J. Yu, T. W. Noh, C. Kim, S.-J. Oh, J.-H. Park, V. Durairaj, G. Cao, and E. Rotenberg, *Phys. Rev. Lett.* **101**, 076402 (2008).
- [24] B. J. Kim, H. Ohsumi, T. Komesu, S. Sakai, T. Morita, H. Takagi, and T. Arima, *Science* **323**, 1329 (2009).
- [25] Y. Okada, D. Walkup, H. Lin, C. Dhital, T.-R. Chang, S. Khadka, W. Zhou, H.-T. Jeng, M. Paranjape, A. Bansil, Z. Wang, S. D. Wilson, and V. Madhavan, *Nat. Mater.* **12**, 707 (2013).
- [26] D. Pesin and L. Balents, *Nat. Phys.* **6**, 376 (2010).
- [27] X. Wan, A. M. Turner, A. Vishwanath, and S. Y. Savrasov, *Phys. Rev. B* **83**, 205101 (2011).
- [28] P. Blaha, K. Schwarz, G. K. H. Madsen, D. Kvasnicka, and J. Luitz, *WIEN2k, Version 13.1, an Augmented Plane Wave+Local Orbitals Program for Calculating Crystal Properties* (Technische Universität Wien, Vienna, Austria, 2001).

- [29] J. P. Perdew, K. Burke, and M. Ernzerhof, *Phys. Rev. Lett.* **77**, 3865 (1996).
- [30] A. I. Liechtenstein, V. I. Anisimov, and J. Zaanen, *Phys. Rev. B* **52**, R5467 (1995); V. I. Anisimov, F. Aryasetiawan, and A. I. Liechtenstein, *J. Phys. Condens. Matter* **9**, 767 (1997).
- [31] The obtained results for the present materials are robust with  $U = 4\text{--}8$  eV for Pr and  $0.7\text{--}2$  eV for Ir, respectively [30]. The  $U$  value of 1.25 eV is chosen for Ir on the basis of a recent first-principles result which reproduces the experimental Mott-insulating state for an isovalent material  $\text{La}_2\text{MgIrO}_6$  to the present material PMIO: G. Cao, A. Subedi, S. Calder, J.-Q. Yan, J. Yi, Z. Gai, L. Poudel, D. J. Singh, M. D. Lumsden, A. D. Christianson, B. C. Sales, and D. Mandrus, *Phys. Rev. B* **87**, 155136 (2013).
- [32] J. Kuneš, P. Novák, R. Schmid, P. Blaha, and K. Schwarz, *Phys. Rev. B* **64**, 153102 (2001).
- [33] G. Kresse and J. Furthmüller, *Phys. Rev. B* **54**, 11169 (1996).
- [34] S. L. Dudarev, G. A. Botton, S. Y. Savrasov, C. J. Humphreys, and A. P. Sutton, *Phys. Rev. B* **57**, 1505 (1998).
- [35] H. J. Monkhorst and J. D. Pack, *Phys. Rev. B* **13**, 5188 (1976).
- [36] A. A. Mostofi, J. R. Yates, Y.-S. Lee, I. Souza, D. Vanderbilt, and N. Marzari, *Comput. Phys. Commun.* **178**, 685 (2008).
- [37] K.-W. Lee and W. E. Pickett, *Phys. Rev. B* **77**, 115101 (2008).
- [38] C. Kittel, *Introduction to Solid State Physics*, 8th ed. (Wiley, Hoboken, NJ, 2005).
- [39] J. Zaanen, G. A. Sawatzky, and J. W. Allen, *Phys. Rev. Lett.* **55**, 418 (1985).
- [40] S. Medling, Y. Lee, H. Zheng, J. F. Mitchell, J. W. Freeland, B. N. Harmon, and F. Bridges, *Phys. Rev. Lett.* **109**, 157204 (2012).
- [41] L. F. Mattheiss, *Phys. Rev. B* **13**, 2433 (1976).
- [42] O. Erten, O. N. Meetei, A. Mukherjee, M. Randeria, N. Trivedi, and P. Woodward, *Phys. Rev. B* **87**, 165105 (2013).